Quenching and electron-irradiation effects in ordered β-PdH(D)$_{0.63}$ around the resistivity anomaly near 50 K

P. Vajda, J. P. Burger, J. N. Daou, and A. Lucasson
Hydrogène et Défauts dans les Métaux, Bâtiment 350, Université Paris—Sud, F-91405 Orsay, France
(Received 22 July 1985)

β-PdH(D)$_{0.63}$ specimens had been quenched across the 50-K anomaly and/or bombarded with electrons of 0.35—0.8 MeV energy at 20 K. They exhibited after each treatment a residual-resistivity decrease, $-\Delta\rho$, which annealed upon heating in the anomaly region. A kinetic analysis of the recovery process yielded an activation energy for H-defect migration of E_m(H,D)$=50\pm15$ meV for a first-order reaction. An investigation of the isotope-dependent radiation-induced $-\Delta\rho_{irr}$ as a function of the electron energy led, by fitting theoretical collision cross sections, to a displacement threshold assimilated with a binding energy of hydrogen in its sublattice, $E_b\sim0.01$ eV, and to a defect resistivity, $\rho_{def}^{H,D}=-6$ $\mu\Omega$ cm/unit concentration. The proposed defect configuration is occupational disorder in the hydrogen-vacancy sublattice, created by site interchange of H atoms with vacant octahedral sites of the Pd lattice. This leads to an effective redistribution of the Ni$_n$Mo ($n=1$—4) type microdomains (Ni equivalent to H, Mo equivalent to H vacancy) as observed by neutron scattering in the anomaly region, by locally forming Ni$_{n\pm1}$Mo-type cells of different symmetry.

INTRODUCTION

β-PdH$_x$ exhibits, for $0.6\lesssim x\lesssim0.8$, a well-known anomaly near 50 K, which had been observed by specific-heat,[1,2] internal-friction,[3,4] and electrical-resistivity measurements.[5,6] In recent years, extensive neutron scattering work has been undertaken (for a review, see Blaschko[7]) which allows one to associate the anomaly with complicated ordering processes involving the interplay of short-range and long-range ordered structures of interstitial H atoms on the octahedral sites of the fcc Pd lattice. It was, in particular, found that samples with higher hydrogen concentrations ($x\gtrsim0.75$) indicated below the anomaly the presence of a Ni$_4$Mo-type structure ($I4/m$ phase),[8,9] while for lower concentrations ($\lesssim0.68$) the hydrogen superlattice had the $I4_1/amd$ symmetry.[10] For intermediate x and for insufficiently relaxed specimens, one obtains mixed domains of various short-range ordered structures of the Ni$_n$Mo type, with $n=1,2,3,4$.[11]

Despite this progress, there remain several unclear points, in particular, the form of the resistivity anomaly (Fig. 1). Thus, the sample resistivity increases upon ordering and a quench leads to a lower residual resistivity value than that of a relaxed specimen.[6] In order to further elucidate these problems, we have undertaken a detailed investigation of the influence of defects introduced into the hydrogen sublattice by quenching and/or by electron irradiation at subthreshold energies for the Pd atoms, and by studying their annealing kinetics. We have, in fact, found that low-temperature irradiation acted in a way analogous to quenching, i.e., by lowering the residual resistivity of the system. The results and conclusions of these studies are presented in the following.

EXPERIMENTAL CONDITIONS

PdH(D)$_x$ specimens were prepared by charging 99.999% pure annealed Pd foils (residual resistivity ratio >500) of 40 μm thickness in an electrolytical bath at room temperature. The loading process was followed resistometrically and was stopped at a concentration corresponding to the compositions PdH$_{0.62}$ and PdD$_{0.63}$, respectively, with a precision of $\pm1\%$. These concentrations are close to the maximum of the resistivity-composition isotherms[12] and correspond to the $(\alpha+\beta)$-β phase boundary at low temperature;[7] they remained stable during the several weeks of the course of the experiment. The specimens had the dimensions $20\times1\times0.040$ mm^3 and were provided with four spot-welded platinum leads for the electrical measurements.

For the irradiations, the samples were mounted in a variable-temperature liquid-helium cryostat connected to

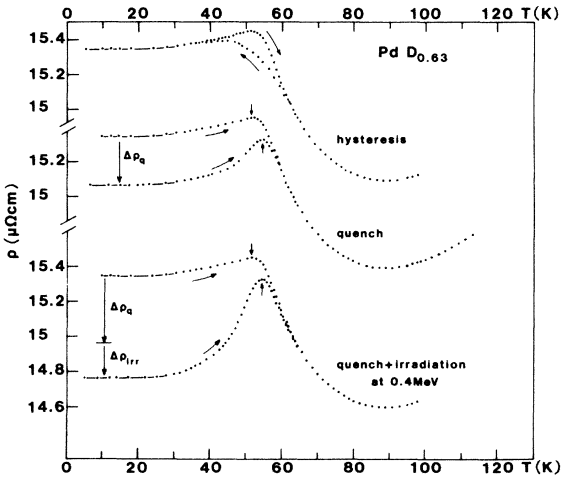

FIG. 1. Resistivity of PdD$_{0.63}$ in the anomaly region, indicating (1) the hysteresis between cooling and heating runs, (2) the effect of a quench, and (3) that of a quench followed by electron irradiation.

a vertical Cockroft-Walton electron accelerator; all of the measurements were done *in situ*. Besides the two hydride samples, a pure Pd-metal foil was placed on the holder and irradiated simultaneously in order to check for possible effects on the metal lattice. No such radiation damage was detected in the energy range 350—800 keV used in the experiment, the displacement threshold in Pd being 34 eV which corresponds to 900-keV incident electron energy.[13]

RESULTS AND DATA ANALYSIS

A qualitative picture of the sample behavior in the region of the anomaly under various treatments is given for $PdD_{0.63}$ through Fig. 1. The uppermost curves show the resistivity of the slowly cooled (relaxed) specimens taken during cooling and in a subsequent heating regime: one notes remarkable hysteresis effects (similar to those described by Herrero and Manchester[14]) indicating relaxation phenomena around the anomaly. The cooling and the heating rates in this run are comparable—of the order of 0.3 K/min. A factor of 30 increase of the cooling rate to 10 K/min led to the quenching effect seen for the intermediate set of curves: the residual resistivity has decreased by $\sim 2\%$ and the introduced $-\Delta\rho_q$ recovers upon heating right in the anomaly region, as has been seen earlier (for example, in Ref. 6). It is interesting to note that a further increase in the cooling rate by a factor of 10^3 did not significantly increase the resistivity change; thus only a $-\Delta\rho_q/\rho_0$ of 2.6% was measured by Senoussi,[15] indicating a relatively low mobility of the quenched species at these temperatures. The lowest two curves show the effect of an electron irradiation at $E=0.4$ MeV performed at $T \lesssim 20$ K and superposed upon a prequenched sample which had been maintained at 4.2 K. The electron bombardment leads to a further decrease of the residual resistivity; when heating the introduced accumulated $-\Delta\rho=-(\Delta\rho_q+\Delta\rho_{\rm irr})$ recovers smoothly in the anomaly region.

Quenching

In this section, we shall analyze the recovery process of the quenched-in $\Delta\rho_q$ from Fig. 1. We show in Fig. 2 the evolution with temperature of $-\Delta\rho_q(T)\equiv\rho_q(T)-\rho_{\rm rel}(T)$, the difference in resistivity between the quenched and the relaxed specimen, for both $PdH_{0.62}$ and $PdD_{0.63}$. Apart from a slight overshoot in the case of the former sample, the behavior is very similar: one clear recovery stage centered near 52 and 54 K for the hydride and for the deuteride, respectively. One can analyze the kinetics of the recovery process of the annealing species by assuming a proportionality between its concentration n and $\Delta\rho_q$, and treating its evolution with time by a chemical rate equation.[16] Thus, for a single activated process with a constant activation energy for migration, E_m, one has

$$\frac{dn}{dt}=K_0 n^{\gamma}\exp(-E_m/k_B T)\,, \tag{1}$$

where K_0 is a reaction constant and γ the reaction order. Working in a constant heating regime (i.e., proportionality between temperature and time, $T=T_0+ct$), we obtain for the migration energy:

$$E_m=-\gamma k_B T_i^2\frac{[d\Delta\rho_q(T_i)]}{dT}[\Delta\rho_q(T_i)]^{-1}\,, \tag{2}$$

by measuring $\Delta\rho_q$ and its derivative at the inflection point T_i (cf. the inset in Fig. 2). The reaction order γ can be determined from Eq. (1) as the slope in a double-logarithmic plot of $d\Delta\rho/dT$ versus $\Delta\rho$. As shall be shown in the next section, it was found that $\gamma=0.9$, indicating a first-order process, for example, random diffusion to a fixed number of sinks. We calculate thus, for the migration energy of the quenched-in defects from the data in Fig. 2:

$$E_m^q(PdH_{0.62})=63\pm 10\ \text{meV}\,,$$

$$E_m^q(PdD_{0.63})=58\pm 15\ \text{meV}\,.$$

Note that these values are the same within experimental accuracy. E_m^q is much lower than the activation energy for hydrogen diffusion as determined from high-temperature measurements, $E_a=0.23$ eV.[17] However, it approaches the value measured in elastic[18] and magnetic[19] aftereffect experiments in the region between 60 and 100 K: $E_a=0.13$ eV; and it becomes comparable to the data taken at $T<60$ K but not evaluated by Higelin *et al.*[19] These authors had attributed both low-temperature activation energies to phonon-assisted tunneling processes.

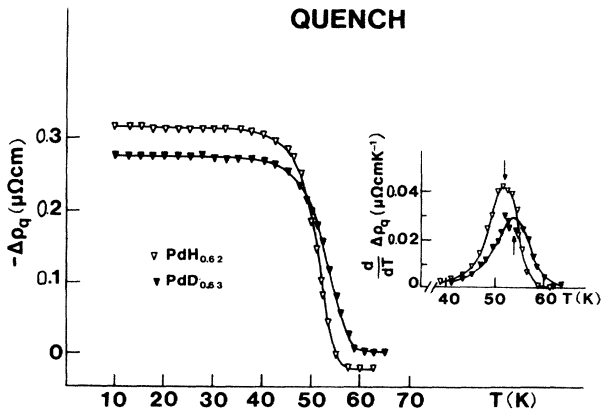

FIG. 2. Recovery of the quenched-in resistivity change $-\Delta\rho_q$ for $PdH_{0.62}$ and $PdD_{0.63}$; the inset shows the derivative of $\Delta\rho_q$ in the annealing region.

Electron irradiation

In Fig. 3 we show the effect of low-temperature irradiation upon the hydride and the deuteride specimens bombarded simultaneously with the same fluence of electrons at various energies in the range 0.35 to 0.8 MeV. One notes a nearly twice as large resistivity decrease in the case of the former sample. This isotope effect is a clear indication of an atomic displacement mechanism involving the hydrogen sublattice as being responsible for the resistivity change, i.e., the production of defects. These defects anneal upon heating in the anomaly region, in the same way as the quenched-in defects, and we shall attempt the same type of kinetic analysis as in the preceding section.

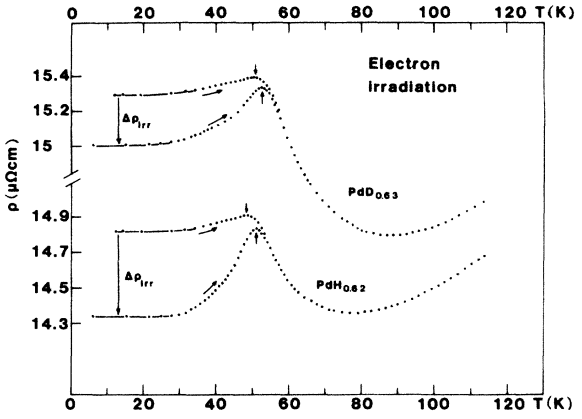

FIG. 3. Resistivity of $PdD_{0.63}$ and $PdH_{0.62}$ before and after electron irradiation at $T \lesssim 20$ K by the same dose, indicating an isotope effect.

Figure 4 demonstrates the recovery of the radiation-induced $-\Delta\rho_{\rm irr}$ as a function of temperature and, in the inset is shown its derivative in the critical region around 50 K. We see again an isotope effect upon the peak temperature, $T_i = 47.5$ K and 50 K for $PdH_{0.62}$ and $PdD_{0.63}$, respectively; both are about 4 K lower than those in the quench experiment. A further distinction is the clear asymmetry of the recovery stage; it begins for $\Delta\rho_{\rm irr}$ already at 30 K, while the $\Delta\rho_q$ did not start to anneal before 40 K, both finishing at about 60 K. (A purely Gaussian behavior has been indicated by dashed lines in the derivative plot in the inset.) Both the lower-peak temperatures and the earlier beginning of the annealing stages indicate a somewhat different defect distribution after electron irradiation when compared to the quenched-in defects. Indeed, the latter reflect a frozen-in situation of the statistical distribution at the quenching temperature above the anomaly (usually ~ 100 K), with an average jump frequency towards annihilation that depends on the total defect concentration. In the irradiation case, however, the transmitted energies in a collision and the number of events per primary incident electron are certainly sufficiently high (as we shall see later in the analysis of the radiation damage) so as to create locally a high density of

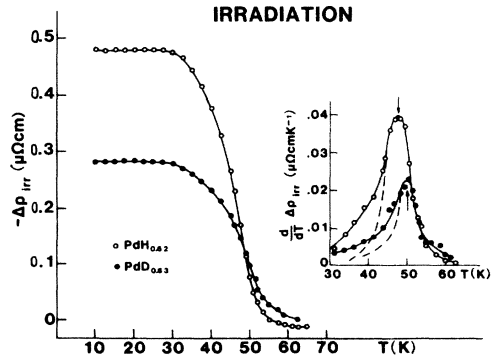

FIG. 4. Same as in Fig. 2, for the radiation-induced resistivity change $-\Delta\rho_{\rm irr}$. The dashed curves indicate a purely Gaussian behavior (see text).

defects, such that the jump frequency needed for recombination is much smaller. Moreover, one can also expect different defect configurations with different binding energies, all this accounting for a deviation from a classical single activated process. Nevertheless, a simple kinetic analysis of the annealing stage seems justified in a first approximation, and we obtain for the migration energies of the irradiation-induced defects

$$E_m^{\rm irr}(PdH_{0.62}) = 40 \pm 10 \text{ meV} ,$$

$$E_m^{\rm irr}(PdD_{0.63}) = 48 \pm 15 \text{ meV} .$$

The activation energies seem somewhat lower than in the case of the quenched-in defects, but are of the same order of magnitude within the experimental accuracy.

Additional information can be obtained by studying the electron-energy dependence of the introduced $\Delta\rho_{\rm irr}$. For sufficiently low defect concentrations (where their interaction can be neglected), one has a proportionality between $\Delta\rho$ and the incident particle fluence, ϕ, thus leading to an expression for the initial resistivity-change rate:

$$\Delta\rho(E)/\phi = \rho_{\rm def}^{\rm H}\sigma_d(E) . \tag{3}$$

Here, $\rho_{\rm def}^{\rm H}$ is the specific resistivity of a hydrogen defect and $\sigma_d(E)$ is the energy-dependent displacement cross section for a hydrogen atom in its sublattice. Thus, by fitting a theoretical σ_d to the experimental data one can hope to obtain a value for $\rho_{\rm def}^{\rm H}$. The results of such a study are shown in Fig. 5 for both the hydride and the deuteride. An immediate and initially somewhat surprising result is the unusual decrease of the resistivity-change rate with increasing electron energy. This is, however, the normal behavior of the atomic displacement cross section, which passes through a maximum, the position of which depends on the value of the energy threshold[20] (see below). As the threshold for displacement of a hydrogen atom

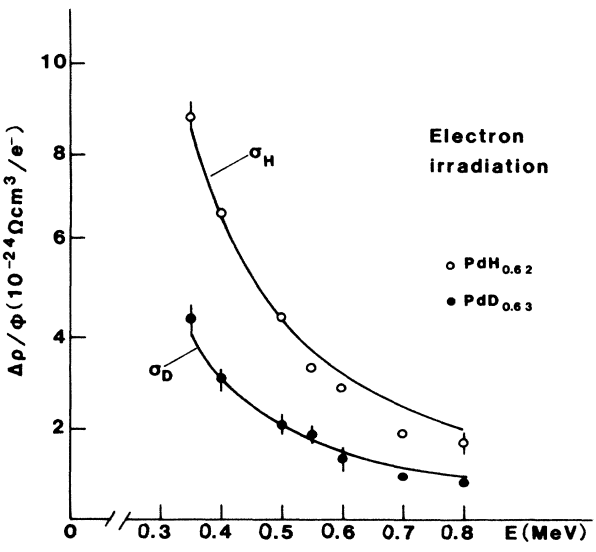

FIG. 5. Initial resistivity-change rates per incident electron for $PdH_{0.62}$ and $PdD_{0.63}$ as a function of electron energy. The drawn curves are calculated displacement cross sections for H and D, normalized at $E = 0.5$ MeV.

from its sublattice site is very low compared to that observed in classical radiation damage studies with metals and intermetallic alloys, we find ourselves also much earlier on the decreasing branch of σ_d than in those cases. For the computation of σ, we have to take into account not only the primary incident electrons but also the secondary electrons created by them during their passage through the sample: $\sigma_d=\sigma_d^{\rm pr}+\sigma_d^{\rm sec}$. One can calculate—as has been done in earlier work with α-LuH_x (Ref. 21)—that the contribution of the secondary electrons (because of their great number which also increases with decreasing energy E) is about 2 orders of magnitude higher than that of the primary electrons. Hence, neglecting $\sigma_d^{\rm pr}$, one can write

$$\sigma_d(E)=\sigma_d^{\rm sec}(E)$$
$$=N_0 t\int_{E_d+I_0}^{E/2}dE'\int_0^{X(E')}dx\int_{T_d}^{T'_{\rm max}}dT'\frac{d\sigma_{\rm MF}(E',T')}{dT'}\frac{d^2\sigma_{\rm el}(E,E')}{dx\,dE'}\,, \tag{4}$$

where N_0 is the number of electrons per cm^3 in Pd and I_0 its mean ionization potential. $d\sigma_{\rm el}/dE'$ is the Møller cross section[22] which gives the number of secondary electrons with an energy E' produced during the passage of a primary electron of an energy E through the sample thickness t. The integral over the secondary-electron range x takes into account their energy loss introducing the stopping power, such that $dx=(dE'/dx)^{-1}dE'$, and the production of further electrons in a cascade process, $d\sigma_{\rm el}/dx$.[23] Now, the stopping power for a keV electron—as already stressed in Ref. 23—is so high that it will interact practically at each lattice site, creating defects and losing energy. The essential energy-loss mechanism being electron excitation, the stopping and the cascade processes will basically compensate each other. $d\sigma_{\rm MF}/dT'$ is the differential scattering cross section for an electron-atom interaction with a transmitted energy T', in the approximation by McKinley and Feshbach.[24] The integrals extend from E_d+I_0 to $E/2$ for the secondary electrons and, for the ensuing energy transfer to the H atoms, from a displacement threshold T_d to $T'_{\rm max}$, the maximum transmissible energy to an atom of mass A,

$$T'_{\rm max}({\rm eV})=\frac{560.8}{A}\frac{E'}{mc^2}\left[2+\frac{E'}{mc^2}\right], \tag{5}$$

where $mc^2=511$ keV; T_d and E_d are related by the same formula (5).

We have calculated σ_d (keeping for the moment T_d as a parameter and normalizing at an intermediate energy $E=0.5$ MeV) and compared it to the experimental data. The fit can be considered as excellent for the energy dependence, underlining the validity of the approximation in Eq. (4). Furthermore, the isotope effect is very well reproduced, which is not surprising as it follows directly through the mass A in the expression for $T'_{\rm max}$. In this calculation we have not taken into account secondary-defect production, since models of the type of that by Kinchin and Pease[25] are hardly justified for a vacancy-rich lattice such as in our system.

More quantitative information can be drawn from Fig. 5 if one succeeds in calculating an absolute value for σ_d. For this, one needs to know the threshold energy for an H-atom displacement, T_d, which can be replaced with a binding energy, E_b, of the H sublattice in the low-temperature ordered state. Now, the latter can be determined from the difference between the actually measured $\rho(T)$ within the thermally activated part of the anomaly region (partially disordered state) and the extrapolated $\rho(T)$ dependence of the low-temperature phase (ordered state) following a Grüneisen-type function for the phononic part of ρ. By fitting a Boltzmann form to this difference,

$$\Delta\rho(T)={\rm const}\times\exp(-E_b/k_BT)\,, \tag{6}$$

one obtains the binding energy as slopes of the straight line in the Arrhenius plot (see Fig. 6):

$$E_b(PdH_{0.62})=13\pm2\ {\rm meV}\,,$$
$$E_b(PdD_{0.63})=16\pm3\ {\rm meV}\,.$$

Entering the above values as T_d in the integral of Eq. (4) one obtains, for example, for $E=0.5$ MeV: $\sigma_d(PdH_{0.62})=1.2\times10^6$ b and $\sigma_d(PdD_{0.63})=0.5\times10^6$ b. A comparison with the experimental $\Delta\rho/\phi$ at 0.5 MeV in Fig. 5 yields immediately from Eq. (3):

$$\rho_{\rm def}^{\rm H}=-3.7\times10^{-6}\ \Omega\,{\rm cm}/0.62\ {\rm at.\ H}\,,$$
$$\rho_{\rm def}^{\rm D}=-4.2\times10^{-6}\ \Omega\,{\rm cm}/0.63\ {\rm at.\ D}\,,$$

giving, in view of the experimental uncertainties, a common value

$$\rho_{\rm def}=-(6\pm2)\ \mu\Omega\,{\rm cm/at.\ H\ (D)}\,.$$

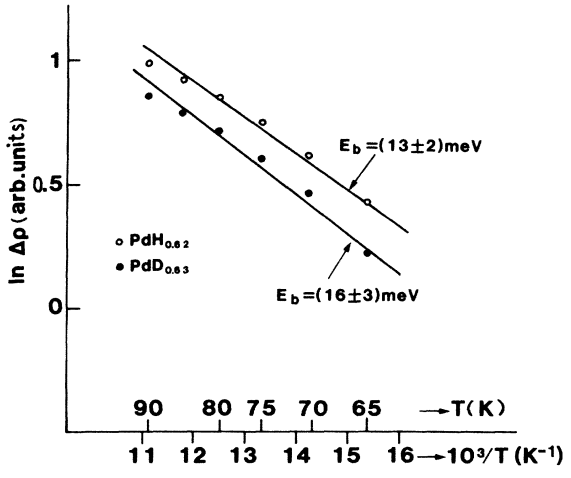

FIG. 6. Determination of the binding energy in the H(D) sublattice by comparing the $\rho(T)$ dependences in the ordered and the disordered states [cf. Eq. (6)].

This value is rather small when compared to a classical point-defect contribution, thus, the vacancy resistivity in the H sublattice of PdH_x was found to be 15 times larger, $\rho_V^H = 85\ \mu\Omega$ cm/unit concentration;[12] here, we are probably dealing with a kind of defect redistribution (cf. also the following "discussion" section) rather than with the introduction of additional interstitial- or vacancy-type defects. Similar effects had been observed earlier in low-temperature irradiated α-LuH_x,[21] where the H-defect resistivity (due to breaking up of a short-range ordered structure) was an order of magnitude smaller than the added hydrogen resistivity itself.

Quench + irradiation

As already done in the case of the quenched and of the irradiated specimens, we present in Fig. 7 the annealing behavior of the prequenched and subsequently electron bombarded $PdD_{0.63}$ sample. An analogous kinetic treatment yielded

$$E_m^{q+\mathrm{irr}}(PdD_{0.63}) = 40 \pm 10 \text{ meV},$$

for a peak temperature of $T_i = 50.5$ K, comparable to the earlier deduced E_m^{irr}. Note also the asymmetry towards lower T, intermediate in importance between the pure quench and irradiation cases, emphasizing the cumulative aspect of the two forms of defect production.

Concluding this section, we shall determine the reaction order γ of the recovery process according to Eq. (1) by plotting $d\Delta\rho(T_i)/dT$ as a function of $\Delta\rho(T_i)$ in a logarithmic graph, for all treatments described previously. From the slope in Fig. 8 one reads

$$\gamma = 0.9 \pm 0.2$$

indicating first-order kinetics.

CONCLUDING DISCUSSION

It is clear from the above presented results that both quench and irradiation introduce point defects in the hydrogen sublattice of the palladium hydride. A quench conserves part of the high-T disordered state of the β phase, while electron irradiation creates an inhomogeneous defect structure at low temperature displacing hydrogen atoms from their regular (sub)lattice site. Their binding energies in the H sublattice, giving rise to a displacement threshold, are $E_b \sim 0.01$ eV; the residual-resistivity change due to the H-defect creation is $\rho_{\mathrm{def}}^{H,D} = -6\ \mu\Omega$ cm/unit. The defects migrate upon heating with an activation energy of $E_m = 0.05 \pm 0.015$ eV (tending rather towards 60 meV for quenched-in defects and towards 40 meV for radiation-induced ones) and recover in the anomaly region in a first-order kinetic reaction.

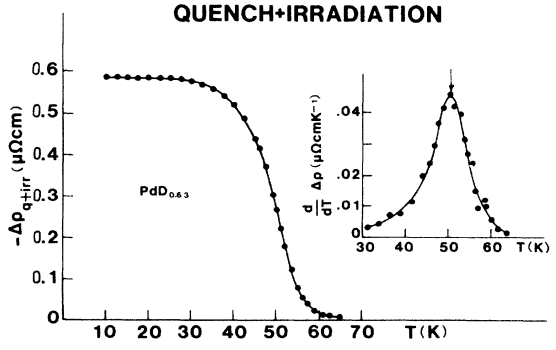

FIG. 7. Same as in Fig. 2, for the (quench + irradiation)-induced $-\Delta\rho_{q+\mathrm{irr}}$ in $PdD_{0.63}$.

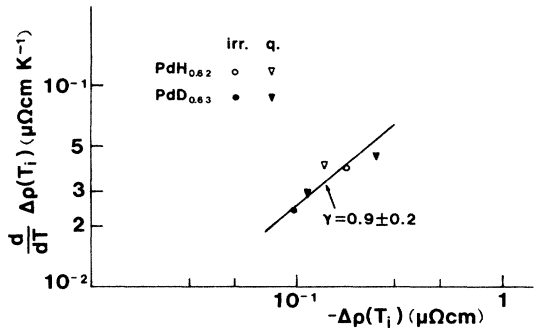

FIG. 8. Reaction-order determination for the annealing kinetics of the H(D) defect after various treatments, cf. Eq. (1).

As to the type of H defect which we are creating in both treatments, it is tempting to suggest a vacancy-type configuration, in view of the particular structure of our substoichiometric hydrides. We have already mentioned in the Introduction the interplay of the different types of Ni_nMo microdomains (discussed by Blaschko[7]) responsible for the lattice distortion. Now, it is easy to imagine that the displacement of an H atom from a regular site will not (or with negligible probability) lead to a Frenkel-type interstitial defect formation such as would be the case in a stoichiometric compound; it will rather push it towards an existing empty site in the neighborhood. This Zener-type exchange mechanism (here, the classical AB alloy is represented by a structure of H atoms and vacancies) has already been used to explain the inelastic damping peaks in internal friction[3] and in ultrasonic attenuation experiments.[26] We want to suggest here that the site interchange between an H atom and vacancy is not just pure hopping as in a classical diffusion process; it leads locally to a change of symmetry in the Ni_nMo microdomain leaving a $Ni_{n-1}Mo$ cell behind and creating a $Ni_{n+1}Mo$ cell in the neighborhood. This change in symmetry results also in a local change of the distortion and, consequently, to a change in electronic structure. Now, as discussed in Ref. 11, the symmetry of NiMo and Ni_3Mo cells is higher (and the distortion lower) than in Ni_2Mo cells. Hence, the originally existing distribution of various Ni_nMo-type cells with a certain mean distortion in the lattice will possibly find itself modified towards a state with, on the average, less distortion and also less perturbation electronically. The latter will quite naturally lead to a lower residual resistivity, thus explaining the unusual behavior upon defect introduction. At the same time, as the number of vacancies in the hydrogen sublattice is conserved in our model, it seems reasonable that the specific

defect resistivity (due to occupational disorder only) should be much lower than a "normal" point-defect contribution (see the preceding section).

A possible explanation for the anomaly form itself can be found in the work of Béal and Friedel[27] from which it follows that the modification of the interference effects between scatterers when local ordering sets in results in an increase of residual resistivity.

ACKNOWLEDGMENTS

Fruitful discussions with O. Blaschko are appreciated. The "Hydrogène et Défauts dans les Métaux" division of the Université de Paris-Sud is "Unité de Recherche Associée au Centre National de la Recherche Scientifique."

[1]D. M. Nace and J. G. Aston, J. Am. Chem. Soc. **79**, 3627 (1957).

[2]J. K. Jacobs and F. D. Manchester, J. Phys. F **7**, 23 (1977).

[3]F. M. Mazzolai, M. Nuovo, and F. A. Lewis, Nuovo Cimento B **33**, 242 (1976); F. M. Mazzolai, P. G. Bordoni, and F. A. Lewis, J. Phys. F **11**, 337 (1981).

[4]G. J. Zimmerman, J. Less-Common Met. **49**, 49 (1976).

[5]N. S. Ho and F. D. Manchester, J. Chem. Phys. **51**, 5437 (1969).

[6]T. E. Ellis, Ph.D. thesis, University of Illinois at Urbana, 1978.

[7]O. Blaschko, J. Less-Common Met. **100**, 307 (1984).

[8]T. E. Ellis, C. B. Satterthwaite, M. H. Mueller, and T. O. Brun, Phys. Rev. Lett. **42**, 456 (1979).

[9]O. Blaschko, R. Klemencic, P. Weinzierl, O. J. Eder, and P. v. Blanckenhagen, Acta Crystallogr. A **36**, 605 (1980).

[10]I. S. Anderson, C. J. Carlile, and D. K. Ross, J. Phys. C **11**, L381 (1978); I. S. Anderson, D. K. Ross, and C. J. Carlile, Phys. Lett. A **68**, 249 (1978).

[11]O. Blaschko, P. Fratzl, and R. Klemencic, Phys. Rev. B **24**, 277 (1981); **24**, 6486 (1981).

[12]J. P. Burger, D. S. MacLachlan, R. Mailfert, and B. Souffaché, Solid State Commun. **17**, 277 (1975).

[13]C. M. Jimenez, L. F. Lowe, E. A. Burke, and C. H. Sherman, Phys. Rev. **153**, 735 (1967).

[14]C. Herrero and F. D. Manchester, Phys. Lett. **86A**, 29 (1981).

[15]S. Senoussi, thesis, University of Paris-Sud at Orsay (France), 1978.

[16]A. C. Damask and G. J. Dienes, *Point Defects in Metals* (Gordon and Breach, New York, 1963).

[17]G. Alefeld and J. Völkl, in *Hydrogen in Metals I*, edited by G. Alefeld and J. Völkl (Springer, Berlin, 1978), p. 321.

[18]R. R. Arons, H. G. Bohn, and H. Lütgemeir, Solid State Commun. **14**, 1203 (1974).

[19]G. Higelin, H. Kronmüller, and R. Lässer, Phys. Rev. Lett. **53**, 2117 (1984).

[20]O. S. Oen, Oak Ridge National Laboratory Report No. ORNL-4897, 1973 (unpublished).

[21]J. N. Daou, P. Vajda, M. Biget, A. Lucasson, and P. Lucasson, Phys. Status Solidi A **40**, 101 (1977).

[22]C. Møller, *Handbook der Physik* (Springer, Berlin, 1958), Vol. 34, p. 56.

[23]W. Dale Compton and G. W. Arnold, J. Appl. Phys. **31**, 621 (1960).

[24]W. A. McKinley and H. A. Feshbach, Phys. Rev. **74**, 1759 (1948).

[25]G. H. Kinchin and R. S. Pease, Rep. Prog. Phys. **18**, 1 (1955).

[26]R. G. Leisure, T. Kanashiro, P. C. Riedi, and D. K. Hsu, J. Phys. F **13**, 2025 (1983); Phys. Rev. B **27**, 4872 (1983).

[27]M. T. Béal and J. Friedel, Phys. Rev. **135**, A466 (1964).